

**Participation of HNO<sub>3</sub> CIMS Instrument in the SAGE III Ozone Loss and Validation  
Experiment (SOLVE)**

NASA Grant No. NAG5-8891  
Georgia Tech Project NO. G-35-623

Final Report

December 1, 1999-November 30, 2000

Submitted to:

NASA Headquarters  
300 E. Street, SW  
Washington, D.C.

Attn: Dr. Philip Decola

Submitted by:

School of Earth and Atmospheric Sciences  
Georgia Institute of Technology  
Atlanta, GA 30332

Principal Investigator: F. L. Eisele

## Final Report

### Participation of HNO<sub>3</sub> CIMS Instrument in the SAGE III Ozone Loss and Validation Experiment (SOLVE)

This project was part of a larger SOLVE project led by Paul Wennberg at California Institute of Technology. The work completed on this project included participating in the installation and preflight testing of a new chemical ionization mass spectrometer for measuring gas and particle phase nitric acid on the ER-2. The investigators subsequently participated in SOLVE where additional instrument improvements were made and a substantial data set was generated. The two Georgia Tech investigators that participated in this work (Fred Eisele and Dave Tanner) had previously been responsible for much of the design and construction of the ion source and mass spectrometer which would be used to measure HNO<sub>3</sub> in SOLVE, with Caltech focusing on inlets, calibration, gas supplies/pumping computer control, and overall integration. Thus, a similar focus remained during the SOLVE measurements though all investigators worked on most if not all aspects of the instrument at some point in the mission. Some of the more interesting results from the study included measurements of nitric acid on what are thought to be 5-20  $\mu\text{m}$  diameter individual particles which could supply a local mechanism for HNO<sub>3</sub> removal.

Nitric acid measurements on SOLVE were completed as a collaborative effort with a great deal of overlap between this project and the larger parent project led by Paul Wennberg. As such, the instrumentation used, its operation, and the resulting measurements are far more fully discussed in the attached report (appendix A) which describes the joint SOLVE nitric acid measurement effort.

## **APPENDIX A**

### **Final Report, NASA / Goddard - Grant NAG5-7527 "Development of an Aircraft-Borne Instrument for Measurement of Nitric Acid"**

P.I. Paul Wennberg, California Institute of Technology. In association with Karena McKinney, Suresh Dhaniyala, and Richard Flagan, Caltech; Fred Eisele, NCAR, David Tanner, Georgia Institute of Technology

A new instrument using chemical ionization mass spectrometry (CIMS) to selectively ionize and detect nitric acid in the stratosphere has been developed in a joint effort at the California Institute of Technology and the National Center for Atmospheric Research. A novel inlet has been developed that is capable of separating, prior to analysis, the aerosol and gas phase nitrate.

#### **Instrument Design**

CIMS has been used to detect  $\text{HNO}_3$  and other acidic and basic atmospheric constituents with high sensitivity and selectivity in ground based and airborne applications (Knop and Arnold, 1987; Schlager et al., 1990; Moehler et al., 1993; Mauldin et al., 1998). Previous CIMS instruments, however, have been ground-based or deployed on large-payload aircraft, such as the P-3 (e.g. Eisele and Tanner, 1991). It was necessary to significantly modify the design for the smaller payload capacity of the ER-2. The CIMS instrument (Figure 1.) discussed here was first deployed on the NASA ER-2 during the SOLVE mission.

### A. Inlet

To quantify nitric acid in both the gas and condensed phases independently, a novel inlet has been designed to enable measurement of volatile species from high-speed aircraft. Bringing particles from outside a high-speed aircraft into aerosol instruments without changing their number or composition is a challenging problem. Previous studies have shown that most existing aircraft inlets have sampling problems (Baumgardner, et al, 1991) and large sampling losses (up to 90%) have been observed in aircraft inlets (Huebert, et al, 1991). For inlets on high-speed aircraft, isokinetic sampling is important not only to maintain representative particle number concentrations in the inlet but also to avoid loss of volatile species from aerosols due to ram heating. Sampling from the ER2 aircraft results in a 20K increase in temperature as the gas stream is brought to rest. This temperature is sufficient to completely evaporate volatile species such as nitric acid from the particles. To estimate gas-phase concentrations, aircraft instruments typically use back-facing inlets that sample from a direction opposite to that of the flow velocity. The contact of the sampled air mass with the cold outer walls of these back-facing inlets results in condensational loss of some sampled species. In addition, recirculation zones at the entrance of these inlets act as particle traps that can contaminate the gas-phase measurements.

For the Caltech/NCAR CIMS instrument, a novel inlet has been designed to enable representative sampling of particles and volatile species without losses and sampling biases. This inlet is operated

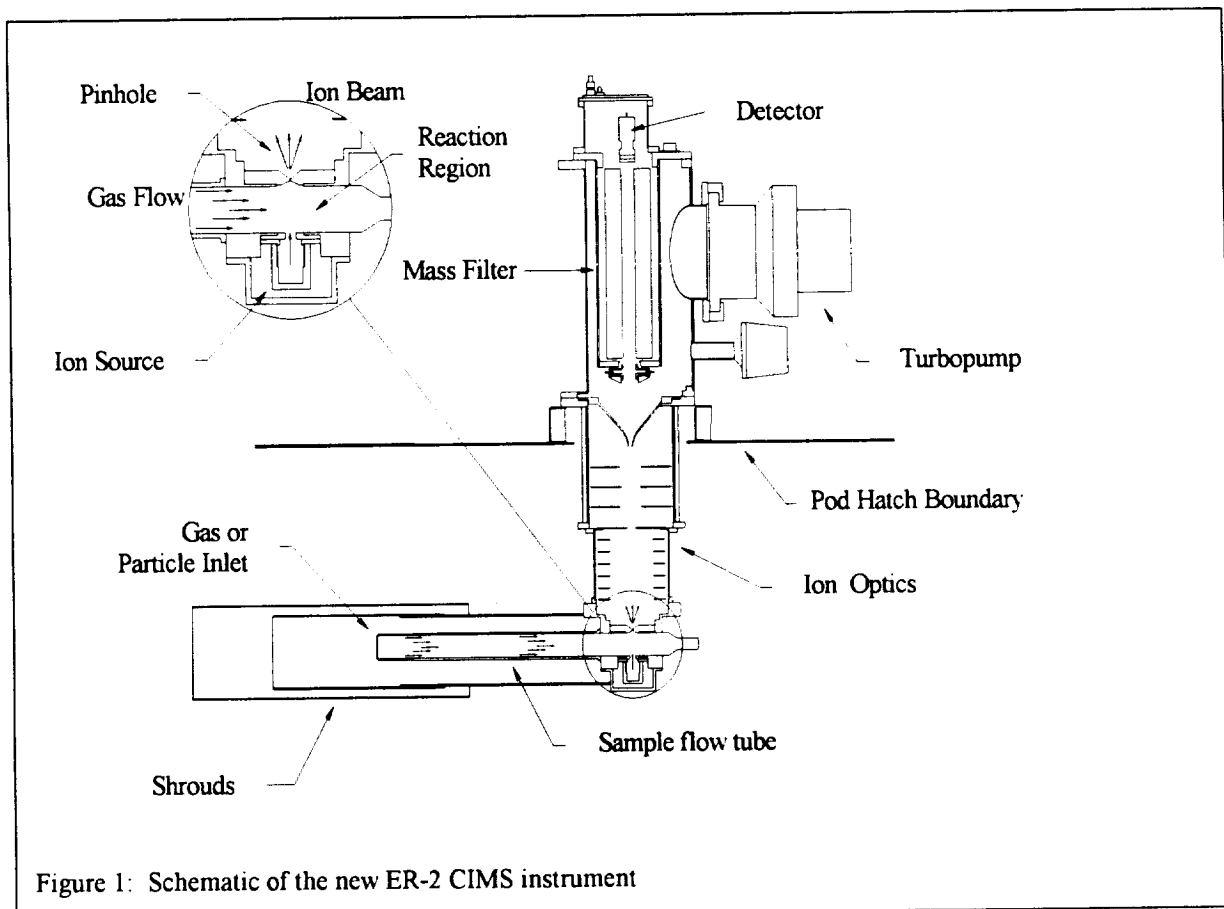


Figure 1: Schematic of the new ER-2 CIMS instrument

in two modes, aerosol mode - to sample aerosols while excluding the gas phase and gas-mode - to sample gas without contamination from the aerosols. Detection of the nitric acid concentration in the sample flow is made following the gas/particle separation by chemical ionization mass spectrometry.

## A.1 Inlet Design

A counterflow impactor technique (Twohy and Rogers, 1993) is used in separating the gas and aerosol phases. Separation of aerosols from ambient flow is possible using the finite inertia of the particles. To collect ambient aerosols, the inlet is operated as an impactor, with the particles impacting onto a clean counterflow carrier gas in the sampler. The counterflow gas excludes the ambient gas, while the particles above a critical size impact through this counter-flowing gas and are carried to the detector. To sample particle-free ambient gas, the gas is brought into the inlet, by sampling perpendicular to the flow streamlines. The non-dimensional number corresponding to particle capture characteristics of impactors is the Stokes number (Hinds, 1982):

$$St = \frac{\rho_p C D_p^2 V}{9 \mu W}$$

where  $\rho_p$  is the particle density,  $C$ , the Cunningham slip correction,  $D_p$ , the particle diameter,  $U$ , the flow velocity towards the impactor and  $\mu$ , the flow viscosity. In conventional impactors, particles with Stokes numbers in the range of 0.3-1.0 and higher are collected on the impactor surface.

To ensure accurate aerosol characterization in the upper troposphere and lower stratosphere, an inlet particle cut size of around  $0.1 \mu\text{m}$  is required. To capture these small particles, a high-velocity jet of narrow width is required. Placing a blunt sampler in free stream, however, results in flow deceleration and streamline deviation well upstream of the impaction region and hence, the sample can capture only the larger particles. Using a multi-stage inlet, however, particles can be brought towards the sampler in a non-decelerated flow enabling a smaller size cut. A cross-section schematic of the inlet design is shown in figure 2. The different components of the designed aerosol/gas inlet are - outer shroud, inner shroud, guide blades, and sampling probe.

The outer shroud is present to ensure that the flow towards the sample probe is unaffected by variations in the incident flow angle due to changes in plane inclination, roll or pitch. Enclosed in the outer shroud is the inner shroud. The inner shroud is made up of two symmetrical sections. Together, these sections have a modified airfoil shape (NASA 63-021) with a long projected "nose" in the front. There are two flow regions allied with the inner shroud - around the outside of the inner shroud; and in the inner channel enclosed by the two half-sections. The flow around the outside of the inner shroud is similar in principle to flow around an airfoil. The flow accelerates as it goes past an airfoil resulting in a region of low static pressure there. The inner shroud is designed such that the region of low pressure lies at the exits of the inner shroud channel. This low pressure ensures that the flow in the inner channel is not decelerated as it approaches the sample probe. The primary flow of interest is the central 10% of the channel flow. This flow is free of wall contact or compressional heating effects. To counter any adverse effect of the boundary layer growth on this central flow, the smooth walls of the inner channel diverge at an angle of  $\sim 4$  degrees.

The appropriate positioning of two small blades in front of the sampling port enables selective aerosol and gas sampling with the inlet. A schematic diagram illustrating the role of these blades,

in aerosol and gas sampling, is shown in figure 1. These blades have thin cross-sections with airfoil-shaped (NACA 0009) leading edges to prevent flow separation. In the aerosol mode, the guide blades are placed symmetrically about the centerline of the sampling probe. As the flow goes past the guide blades, it accelerates at the downstream end resulting in a region of low pressure. This low-pressure region provides the suction required forming an accelerated jet between the guide blades directed towards the sample probe. This high-velocity jet enables the impaction of small particles onto the counterflow gas coming out of the sample probe.

In the gas-mode, one of the blades is moved forward by a stepper motor to occlude the sampling port and to enable particle-free ambient gas to enter the sample probe. The low pressure regions at the downstream end of the guide blades provides the "boundary-layer" suction that removes the ambient gas in contact with the walls of the blades. Also, the shape and position of the guide blades is optimized to ensure that there are no recirculation zones in the vicinity of the sampling port.

The sample probe has a slit opening through which sampled gas or particles are brought in. A set of opposing jets is introduced through channels just downstream of this slit opening. The gas introduced here primarily acts as a carrier gas for transporting the sampled particles towards the detector with a small excess amount used as the counterflow gas.

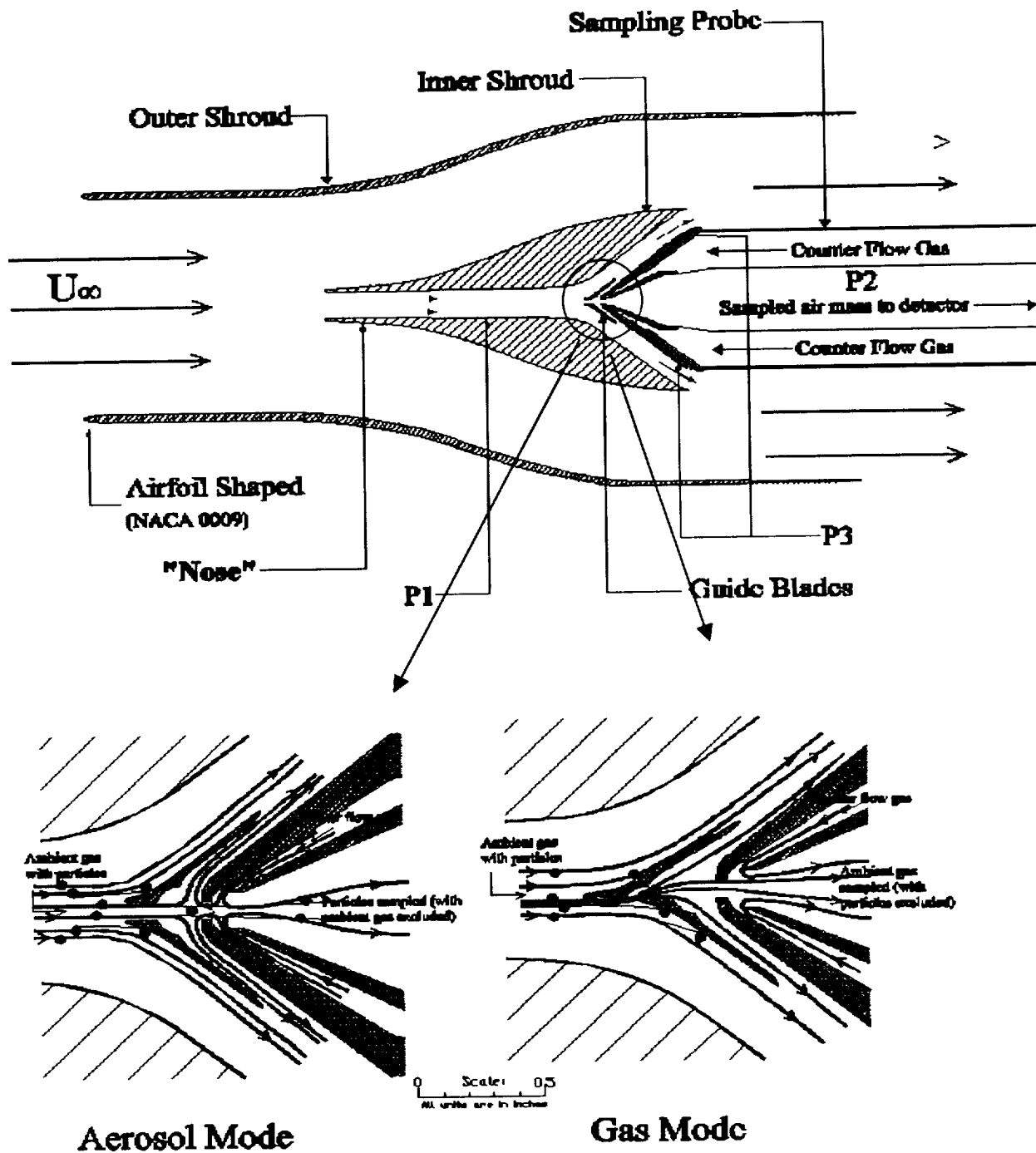


Figure 2: Top panel: Schematic showing the different components of the CIMS inlet – outer shroud, inner shroud, guide blades, and the sampling probe. Bottom panel: The operation of the inlet in the aerosol mode (left) and the gas mode (right) is shown. The counterflow gas keeps the gas out of the sample in the aerosol mode, while in the gas mode, the positioning of the blades is optimized to ensure the gas sample is free of particles and wall-contact. The slit opening is 2 mm.

## A.2 Inlet Simulations

Flow simulations using computational fluid dynamics (CFD) tools have been used to arrive at the final inlet design. Commercial CFD software, FLUENT, has been used in this flow modeling. This code is based on a control volume technique (Patankar, 1980) and has been used in similar flow conditions by other researchers. For use of the inlet on a high-speed, high-altitude aircraft, the flow regime to be modeled is compressible and turbulent and k- $\epsilon$  viscosity model is used for the turbulence simulations.

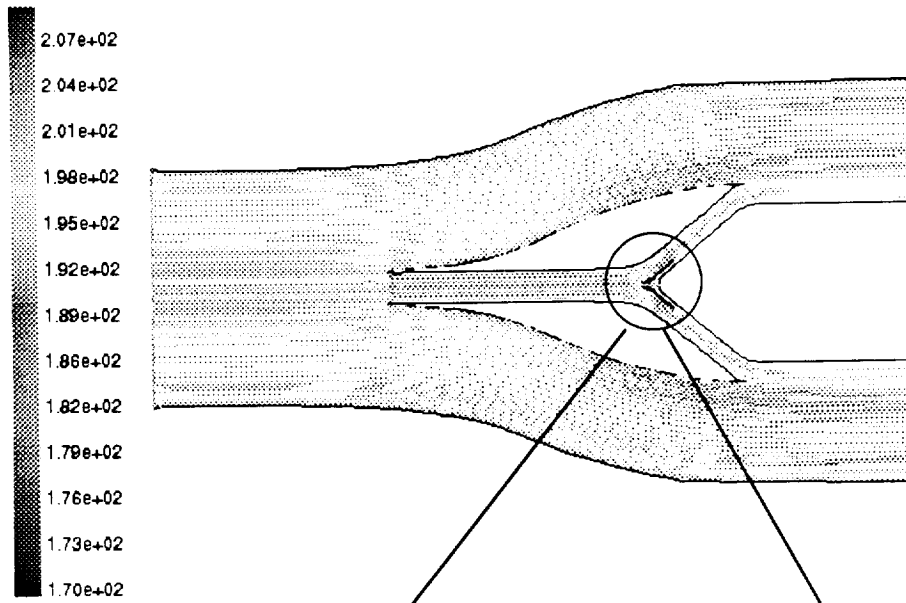
The geometry of the inlet and the shroud is inherently three-dimensional. However, two-dimensional flow modeling is seen to capture the inlet performance without loss of accuracy and this has been verified by comparing the results of the 2D modeling with that obtained using a 3D domain. In both, 2- and 3D modeling, symmetry boundary conditions are used whenever possible to reduce computational domain.

The use of airfoil-shaped edges at the shroud tips prevents flow separation at the entrance. The thin cross-sections of these edges are seen to prevent distortions of flow streamlines and particle tracks, as they enter the outer shroud. Typical simulation results showing streamlines in the outer shroud are shown in figure 3a. The flow heading towards the sampler passes through the different inlet stages without distortions or compressional heating. Flow simulations have been performed at various angles of attack (upto 14 deg), and the outer shroud is seen to effectively straighten the flow and the particles headed towards the inlet. The inlet is, therefore, insensitive to the normal aircraft orientation and maneuvers.

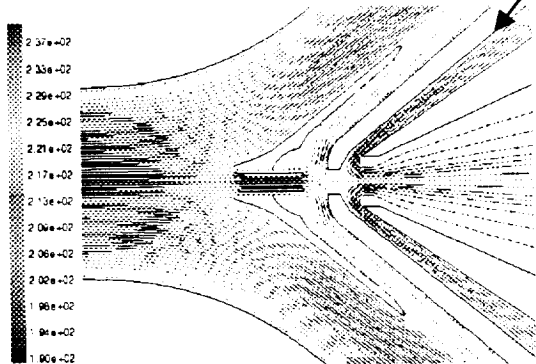
The flow around the inner shroud accelerates as it goes past the downstream end, producing a low-pressure region. This low-pressure region provides the suction for the flow in the channel enclosed by the inner shroud. The flow in the channel accelerates and reaches close to sonic velocities producing the cold flow temperatures in the inner shroud channel. The accelerating flow also results in the channel static pressure being somewhat less than the ambient static pressure. The presence of the long "nose" at the front-end of the inner shroud prevents streamline deviations in the flow entering the channel. Therefore, the inner shroud transports the ambient gas and particles towards the guide blades without altering their composition.

## A.3 Aerosol Mode

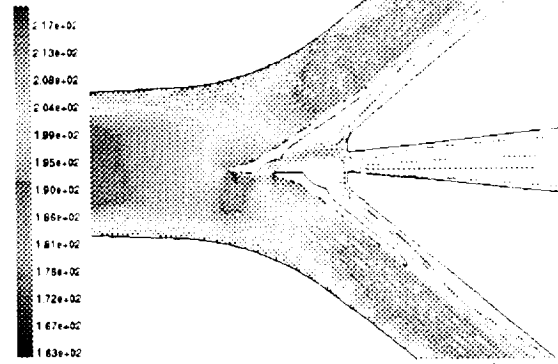
The streamlines near the guide blades, positioned symmetrically about the sample probe centerline for aerosol sampling, are shown in figure 3b. The shape and position of the guide blades results in a high-velocity, narrow width jet directed at the sample probe. Particles do not experience any heating prior to their impaction onto the counterflow gas. The tracks of 0.7 $\mu$ m diameter particles near the guide blades are shown in figure 3d. The particle tracks are calculated by solving for the Stokes' drag on the particle and the slip correction is applied considering the local pressure. The flow conditions created by the inner shroud and the guide plates result in effective collection of these particles.



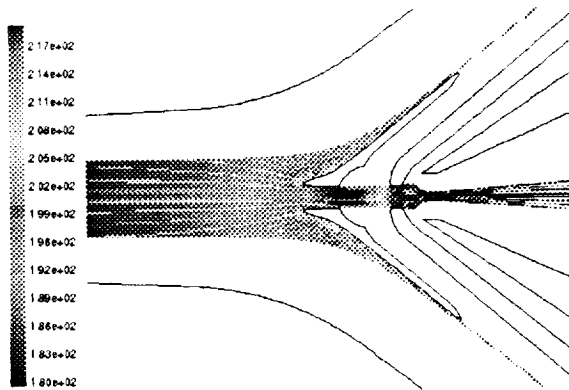
(a) Flow streamlines inside the outer shroud of the inlet.



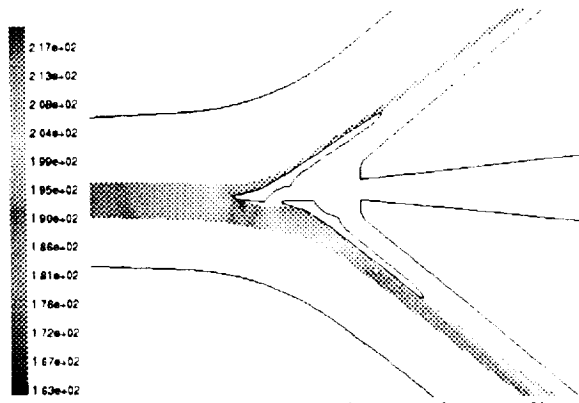
(b) Aerosol mode operation – Streamlines near the sampling port, colored by flow temperature



(c) Gas mode operation - Streamlines near the sampling port, colored by flow temperature



(d) Aerosol operation – Particle tracks near the sampling port, colored by particle temperature.



(e) Gas mode – Particle tracks near the sampling port, colored by particle temperature.

Figure 3: Flow and particle simulation results for the inlet operating in the aerosol and gas sampling modes

#### A.4 Gas Mode

The streamlines in the gas-mode case are shown in figure 3c. The tracks of  $0.3 \mu\text{m}$  diameter particles (figure 3e) show that the particles sampled in the aerosol mode are not sampled in the gas mode. The low-pressure regions downstream of the guide blades provide the required "boundary layer" suction to enable sampling of gas streamlines without any wall contact. Also, the guide blade design ensures the absence of recirculation zones near the sampling region.

The collection efficiency curves are obtained by simulating particle tracks of different sizes in the two modes of the inlet operation (figure 4). The particle collection efficiency of the inlet in the two modes has small pressure dependence over the range of interest here. The particle-cut size for the inlet in the aerosol mode is around  $0.2 \mu\text{m}$ , while particles larger than  $0.1 \mu\text{m}$  are not sampled in the gas mode.

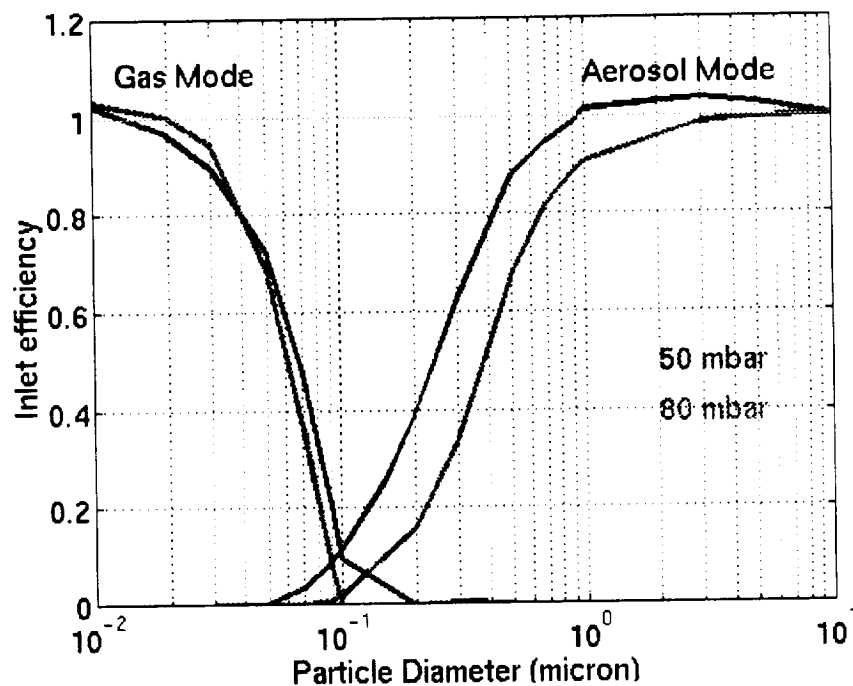


Figure 4: The particle collection efficiency curves for the inlet operated in the two modes for different ambient pressure.

#### A.5 Experimental Tests

The primary performance test of the inlet is the comparison of inlet pressures obtained from simulations with the in-flight inlet pressure measurements. The different pressure measurements made in the inlet are at - inner shroud channel, inside the sampling probe and at the exit of the inner shroud. The locations of the pressure probes are marked in figure 2 as P1, P2 and P3 respectively. In the inner shroud channel, pressure measurements using a static pressure probe are obtained to monitor the inlet performance.

A plot of these static pressures as a function of ambient pressure is shown in figure 4a. Also plotted in this figure are the static pressures obtained from CFD simulations. As predicted, static pressures in the channel are lower than the ambient pressures. There is however, a ~10% discrepancy between the measured and predicted channel static pressures. The results of 3D simulations are similar to that obtained from the 2D simulations, indicating that this difference is not likely due to 3D effects. In the sample probe, the pressure measurements differ in the two operational modes of the inlet. In the aerosol mode, the pressure in the sampling probe is the flow stagnation pressure. This pressure can be compared with the in-flight measurements of total pressure and the comparisons are plotted in figure 5b. The measurements of total pressure are in good agreement with the predicted values indicating that there is no loss of pressure-head in the inner shroud channel. The flow calculations based on the measured total and static pressures indicate that the velocity in the channel is greater than the cruise velocity of 0.7 Mach and hence, the particles do not experience compressional heating in the inlet channel. In the gas mode, the sample probe pressures are lower than the ambient as predicted in the simulations (figure 4b). However, the measurements and predictions are also different by about 10%. The 10% discrepancy is likely due to the absence of the pod and the wing in our simulations. However, sensitivity simulations of inlet performance show that the inlet particle-capture characteristics are not very sensitive to small changes in channel velocities.

## A.6 Gas Flow Rate and Temperature Control

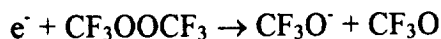
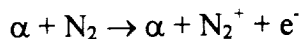
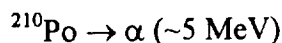
While sampling in either gas or particle mode, dry nitrogen gas can be added to the inlet near the sampling slit. The nitrogen flow rate can be adjusted from zero to slightly greater than the total flow through the inlet, which results in a net outflow of gas from the inlet. In aerosol mode, this 'counterflow' serves to exclude ambient gas from the sample, while providing a carrier gas for the sampled particles. In normal gas mode operation, the counterflow is zero, however, setting the counterflow to inlet flow ratio to greater than 1 while in gas mode allows exclusion of the ambient air as well as particles, and determination of the nitric acid background. In both modes, the inlet geometry coupled with the impinging counterflow just inside the inlet causes the flow to be turbulent and well mixed in this region. This assists in homogenizing the flow.

After entering the inlet, the ambient gas or particle sample passes through a 2.5-cm diameter flow tube 30 cm long before reaching the detection region. The velocity in the flow tube is controlled by a positive feedback loop in which the mass flow rate and pressure are monitored and used to modulate the speed of a small roots pump. Typically, the velocity in the flow tube was maintained at  $0.7 \text{ m s}^{-1}$ , resulting in a residence time in the flow tube of 0.43 s. The flow is heated to  $\sim 290 \text{ K}$  by contact with the tube walls, and the sample gas temperature is monitored at several locations along the flow tube. At this temperature, nitric acid condensed on particles is rapidly evaporated into the gas phase before reaching the detection region. The heated, PFA-coated walls also minimize nitric acid loss by condensation on the flow tube surfaces.

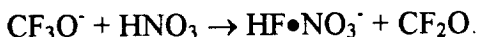
## B. Ion Source and Ion Sampling

We have developed transverse ion source, in which the source is located directly across the flow tube from the mass spectrometer inlet (Mauldin et al., 1998). This geometry is advantageous because the ion-molecule reaction time is independent of the flow rate through the sample tube. Ions produced in the ion source are directed across the sample flow by electrostatic lenses positioned at the ion source outlet and at the inlet to the mass spectrometer. The ion-molecule reaction time is determined by the gas pressure, the distance across the flow tube (2.5 cm), and the potential difference between the lenses. Under typical flight conditions, this results in a reaction time of  $\sim 2 \text{ ms}$ . By controlling the reagent ion and reaction time, the ion-molecule reaction can occur in either a kinetic or equilibrium regime, allowing optimization of the ionization chemistry for many different species.

$\text{CF}_3\text{O}^-$  was chosen as the reagent ion for nitric acid detection. The reactions of this ion with many minor atmospheric constituents have been studied by Huey et al., (1996). The reaction rate of  $\text{CF}_3\text{O}^-$  with nitric acid was shown to be very fast ( $k=2.2 \times 10^{-9} \text{ cm}^3 \text{ molecule}^{-1} \text{ s}^{-1}$ ), and the product of the reaction,  $\text{HF} \cdot \text{NO}_3^-$ , was not observed in the reactions of  $\text{CF}_3\text{O}^-$  with other atmospheric traces species that were tested. The reagent ion is formed in a multi-step process by passing reagent ion precursors, in this case  $\sim 2 \text{ ppmv}$  of  $\text{CF}_3\text{OOCF}_3$  in nitrogen at a flow rate of 100 sccm, over a  $^{210}\text{Po}$  alpha source. The ion generation scheme is as follows:



The reagent ions are directed out of the ion source, and across the sample flow, where nitric acid reacts with the precursor ion:



Observed product ion intensities vs. ion-molecule reaction time show that the reaction is in a kinetically controlled regime. Under these conditions, the ratio of product ion to reagent ion can be related to the nitric acid concentration by:

$$[\text{HNO}_3] = -\frac{1}{kt} \ln \left( 1 + \frac{[\text{HF} \cdot \text{NO}_3^-]}{[\text{CF}_3\text{O}^-]_0} \right)$$

where  $k$  is the ion-molecule reaction rate constant, and  $t$  is the reaction time. For  $k$  and  $t$  as given above, and typical stratospheric flight conditions, where the nitric acid concentration is  $\sim 2 \times 10^{10}$  molecules  $\text{cm}^{-3}$ , the expected product ion to reagent ion ratio is about 0.1.

### C. Mass Spectrometer

Ions in the reaction region are directed by the electrostatic lenses through an aperture into the vacuum system. The aperture size is adjusted to maintain a constant mass flow of gas into the vacuum system over the altitude and pressure range of interest. The ions and a small amount of gas are expanded into first stage of the vacuum system, known as the collisional dissociation chamber. During the expansion and coincident cooling, it is possible for the ions to form clusters with condensable gases. This chamber is maintained at a pressure of  $\sim 0.1$  mbar by a critical orifice between the first and second stages. The ions are accelerated towards the second stage by a small electric field. Due to the high pressure in this chamber, collisions between ions and the surrounding gas can result in ion fragmentation. Fragmentation and de-clustering can be controlled by tuning the electric field such that the larger, less tightly bound clusters formed in the expansion are broken up in the collision chamber, but the product ion remains intact.

From the collision chamber, ions enter a differentially pumped concentration region at a pressure of  $10^{-3}$  mbar. Of the total gas flow of approximately 25 sccm into the chamber, 99% is pumped away directly, and only 1% of the gas passes into the final stage with the ions, providing a factor of 100 increase in ion concentration. Ion optics in this chamber focus the ions into a beam along the central axis. A beam skimmer allows only those ions with trajectories within a limited acceptance angle into the final chamber. The final stage of the vacuum system houses additional focussing lenses and the mass filter. A second pump maintains the pressure at  $10^{-5}$  mbar. The quadrupole mass filter (Extrel) employs 19

mm diameter rods, and operates a resolution of 0.5 amu over a mass range of 10 to 250 m/z. The RF power supply and control electronics for the mass filter is a commercially available unit (Extrel) modified to operate at low ambient pressures. The mass spectrometer can be programmed to operate in mass scan mode, or can integrate a single mass peak over time. Following mass selection, ions are detected by a channel electron multiplier (K & M Electronics) operating in pulse counting mode.

The vacuum system is pumped by two 250 L/s turbomolecular pumps (Varian). They are backed by a sorption pump containing molecular sieve 5A, and cooled with liquid N<sub>2</sub>. The sorption pump provides the required backing pressure for the turbopumps, and approximately 10<sup>5</sup> mbar-L of pumping capacity, adequate for a 12-h flight. Clean nitrogen boil-off from the liquid is used for the inlet counterflow gas. Pressure in the intermediate stage of the vacuum system (10<sup>-3</sup> mbar, nominal) is monitored with a Pirani gauge (Wenzel Electronics) with an operating range of 10<sup>3</sup> – 10<sup>-5</sup> mbar. This sensor is used in a feedback loop to control the adjustable aperture at the entrance of the collisional dissociation chamber, thereby controlling the vacuum system pressure and mass flow rate.

#### D. Calibration

In theory, in an ideal system where the ion-molecule chemistry is well characterized, the nitric acid concentration can be determined from the ratio of the product and reagent ions, as described by Equation 1. However, complication of the kinetics by other reactions, and variations in instrument performance (such as ion intensity and inlet flow conditions), make an independent calibration method essential. Accordingly, a constant amount of isotopically labeled H<sup>15</sup>N<sup>18</sup>O<sub>3</sub> is added to the sample. The calibration gas is delivered by a permeation tube containing liquid H<sup>15</sup>N<sup>18</sup>O<sub>3</sub> installed in a temperature, flow, and pressure controlled cell, through which dry nitrogen is flowed at a rate of 50 sccm. The calibration pressure control system was designed such that all control devices are located upstream of the permeation tube, with only teflon tubing, glass critical orifices, and a single bypass valve downstream of the calibration source. This configuration minimizes loss of the calibration gas prior to delivery to the inlet. A phase change material is used in the calibration system to insure that temperature control remains, even when the instrument is power off for several hours (for example during fueling of the aircraft). The absolute concentration of labeled nitric acid in the flow was determined absolutely by periodically collecting the output by bubbling it through water, and analyzing the resulting sample by ion chromatography. When possible, the permeation rate of the calibration tube was verified by determining the change in mass over time.

The calibration gas is added to the sample flow tube just downstream of the inlet so that the calibration gas is well mixed into the sample flow, and is exposed to conditions identical to those of the ambient sample prior to detection. Use of isotopically labeled nitric acid allows continuous addition of the calibration gas, providing maximum stability of the calibration, and minimizing hysteresis effects due to variations of the calibration gas. The calibration gas is periodically pumped away during flight for short periods of time to determine its background level.

Table 1. ER-2 CIMS Instrument Weights and Locations

INSTRUMENT		Weight (Lbs)	PS	CG Location*	
				WL	CL
MASS SPECTROMETER	(actual)	42.50	455	79	7
INLET ASSEMBLY (including stiffening)	(actual)	13.20	448	69	-11
STRUCTURE, INSTRUMENT	(actual)	21.00	465	84	0
GAS HANDLING ASSY.	(actual)	21.50	470	90	-3
DEWAR/SIEVE PUMP (FULL)	(est)	43.00	525	95	0
FLIGHT COMPUTER	(actual)	7.00	479	89	3
RF POWER SUPPLY	(actual)	11.00	447	86	-3
TURBO PUMP CONTROLLER	(actual)	5.00	447	89	5
MAIN POWER SUPPLY	(actual)	9.80	480	79	0
INLET INTERFACE CONTROLLER	(actual)	3.50	454	91	5
DEWAR SUPPORT	(est)	1.50	520	89	0
CABLES	(actual)	10.00	480	89	0
<b>TOTAL INSTRUMENT</b>		<b>189.00</b>			
<b>CG LOCATION OF INSTRUMENT</b>			<b>477</b>	<b>86</b>	<b>1</b>

\* Locations refer to ER-2 stations

#### E. Support electronics and Engineering Information

Additional instrument components include repackaged commercial turbopump controllers (Varian), temperature and motor controllers for the inlet components, and a gas handling system for the inlet flows. The instrument is controlled by a single board computer with an AMD 5x86 processor (Teknor), interfaced to PC104 data acquisition boards (Diamond Systems, Oregon MicroSystems). All instrument operation during flight is automated, with specific stages of power-up and power-down triggered by an ambient pressure transducer. The instrument is entirely powered by 28 VDC power available on the ER-2. A central power conversion and distribution unit supplies the required voltage to each instrument component. Typical instrument power consumption during flight is 800 W, 1200 W maximum.

The CIMS instrument is controlled with software developed under contract to Norton Allen. Control operation within the QNX operating system and the proprietary software worked flawlessly during SOLVE.

For SOLVE, the CIMS instrument was located in the right superpod midbody. The instrument was attached to the structural members of the midbody hatch cover, with the inlet protruding through an opening in the hatch skin. This configuration significantly simplified the instrument installation and maintenance. By mounting the instrument on a removable section of the aircraft pod, the entire instrument could be up- or downloaded by simply installing the hatch cover, thereby avoiding the need to remove the inlet from the instrument for each installation. The liquid nitrogen dewar / sorption pump assembly was mounted remotely in the tail cone of the right superpod, and coupled to the vacuum

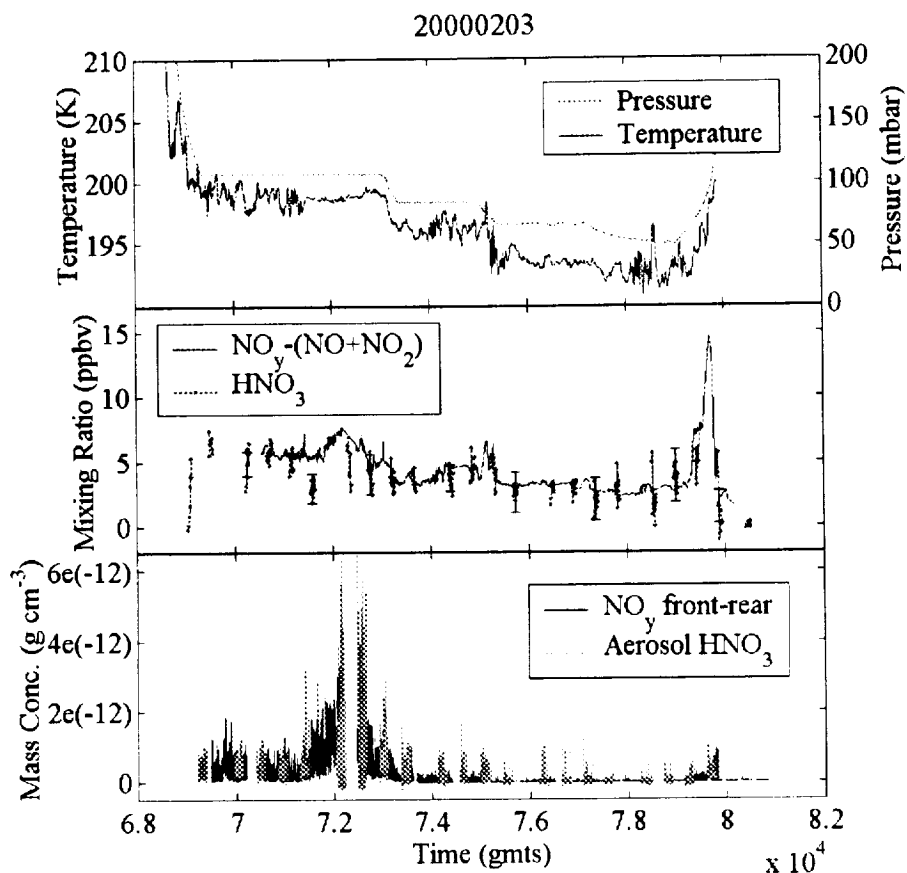


Figure 6: Data from the ER-2 flight of February 3, 2000: (Top panel) pressure and temperature. (Center panel) Gas-phase CIMS  $\text{HNO}_3$  ( $2\sigma$  precision error bars) and  $\text{HNO}_3$  estimated from  $\text{NO}_y$  measured at the rear inlet. (Bottom panel) Aerosol-phase CIMS  $\text{HNO}_3$ , shown with  $\text{NO}_y$  front inlet measurements for comparison.

system with a large diameter teflon vacuum hose. By locating the dewar to the aft of the main components, the center of gravity of the instrument was moved further aft, satisfying a constraint on the second moment of the combined pod payloads, and permitting a greater overall weight budget. The weights of the individual CIMS instrument components, as well as their locations and an analysis of the center of gravity for the SOLVE configuration are provided in Table 1.

## Instrument Performance

### A. Typical Operation

During a typical ER-2 flight, the instrument is activated by an ambient pressure switch when pressures below 300 mbar are reached. Following vacuum system pump-down, the mass spectrometer is turned on and the variable aperture into the vacuum system is opened. The instrument is cycled between gas and aerosol modes with a cycle time of 6 minutes. The inlet flow and counterflow rates are adjusted to maintain a constant flow tube velocity in both modes. In gas mode, the counterflow is set to 1.5 times the total inlet flow to determine the nitric acid background, and then set to zero to measure nitric acid in the ambient air sample. In aerosol mode, the counterflow is varied between three settings, 0.4, 0.7, and 1.5 times the total flow, to assure complete sampling of condensed nitric acid with and without excess counterflow. The values obtained with counterflow ratios of less than 1 are later corrected using the gas mode data.

Within each measurement mode, the mass spectrometer is dithered between the reagent ion, product ion, and calibration product ion mass peaks, as well as several other diagnostic mass peaks. In addition, during several flights, product ion peaks for other detectable atmospheric species, such as HCl and H<sub>2</sub>O were monitored. Although these species were not quantified, non-zero signals were observed, and we expect to detect these species quantitatively after improving the sensitivity through further developmental work.

At longer time intervals (every 4 complete gas/aerosol mode cycles, or about 0.5 h), a calibration cycle was run, in which the mass spectrometer was scanned from  $m/z = 10$  to 125, and the mass scale was recalibrated to the reagent ion maximum signal. This compensated for a slight mass drift observed due to temperature change of the mass spectrometer electronics. We were also able to look for possible product or interference peaks in the mass spectrum. The mass scan was followed by a calibration background test, in which the calibration gas flow to the inlet was turned off, allowing an assessment of the calibration gas background and the time constant for nitric acid retention in the inlet.

### B. Performance

The CIMS instrument successfully measured nitric acid on all but two ER-2 flights during SOLVE. The data from the flight of February 3, 2000, is shown in Figure 6. Gas-phase HNO<sub>3</sub> observed by CIMS ( $2\sigma$  precision error bars) is plotted in the center panel. Because the CIMS instrument alternated between gas and aerosol modes during flight, gas phase data is reported for approximately half of the total flight time. By improving the ion throughput of the mass spectrometer and optimizing the product to reagent ion ratio, we improved the instrument precision from 1 ppbv in 7 s for the first ER-2 deployment (20000115 to 20000205) to 0.3 ppbv in 7 s for the second deployment (20000223 to 20000316). The accuracy of the gas phase measurements is estimated to be  $\pm 25\%$ ,  $\pm 1$  ppbv.

In Figure 6, the CIMS measurements are compared with  $\text{HNO}_3$  estimated from  $\text{NO}_y$  measured by the NOAA Aeronomy Lab instrument (Fahey et al., 1989) at the rear inlet by subtracting small contributions from  $\text{NO}$ , and  $\text{NO}_2$  measured simultaneously.  $\text{ClONO}_2$ , which also contributes to  $\text{NO}_y$ , was not reported for this flight, however it is estimated to be a few hundred pptv or less, as is  $\text{N}_2\text{O}_5$ , which was not measured. There is also a contribution to  $\text{NO}_y$  measured at the rear inlet due to the sampling of small ( $<2 \mu\text{m}$ ) particles, which has not been removed. There is good agreement between the CIMS  $\text{HNO}_3$  measurements and the  $\text{NO}_y$  measurements, as expected under chemically perturbed Arctic vortex conditions where  $\text{HNO}_3$  is the major component of  $\text{NO}_y$ . Figure 7 shows a direct comparison between  $\text{HNO}_3$  measured by CIMS in the gas phase, and that determined from simultaneous measurements of  $\text{NO}_y$ ,  $\text{NO}$ ,  $\text{NO}_2$ , and  $\text{ClONO}_2$  for six vortex flights during SOLVE. Gas-phase nitric acid from the two methods agrees to within the uncertainties of the measurements for these flights.

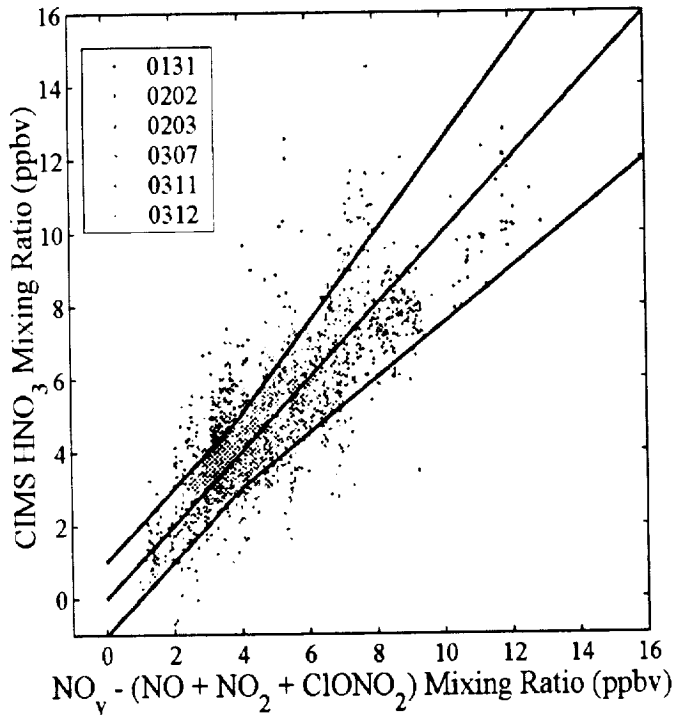


Figure 7: Comparison of gas phase  $\text{HNO}_3$  measured by CIMS with that derived from  $\text{NO}_y$ ,  $\text{NO}$ ,  $\text{NO}_2$ , and  $\text{ClONO}_2$  measurements. The bounds on either side of the central 1:1 relationship are the greater of  $\pm 25\%$  of the value, or  $\pm 1$  ppbv.

Aerosol-phase CIMS measurements of  $\text{HNO}_3$  for the February 3 flight are shown in the lower panel of Figure 6. Also shown are the difference between the  $\text{NO}_y$  front inlet and rear inlet measurements for comparison. Because the  $\text{NO}_y$  front inlet samples the gas phase plus all particle diameters, whereas the rear inlet samples the gas phase plus particles up to  $2 \mu\text{m}$  diameter, the difference between the two channels is a good estimate of  $\text{NO}_y$  on particles larger than  $2 \mu\text{m}$ . Between 39000 and 46000 gmts, both instruments

show an increase in size and frequency of short duration peaks in nitric acid. These features have been interpreted as the sampling of large (5 to 20  $\mu\text{m}$ ) individual nitric acid-containing particles. Statistical analysis of the measurements, which accounts for the instrument sampling volumes and responses, shows that the two data sets are consistent with the same ambient particle size distribution.

In aerosol mode, the single particle detection limit was  $1 \times 10^{-13} \text{ g cm}^{-3}$  for the first deployment, and  $0.2 \times 10^{-13} \text{ g cm}^{-3}$  for the second deployment, corresponding to approximate particle diameters of 7  $\mu\text{m}$  and 5  $\mu\text{m}$  (assuming NAT), respectively. The average detectable aerosol mass concentration was  $1 \times 10^{-14} \text{ g cm}^{-3}$  (0.05 ppbv) and  $0.4 \times 10^{-14} \text{ g cm}^{-3}$  (0.02 ppbv) for a 7-s integration period for the two deployments. Instrument accuracy is  $\pm 25\%$ ,  $\pm 2 \times 10^{-14} \text{ g cm}^{-3}$  (0.1 ppbv) for aerosol mode.

### C. Future Plans

Currently, efforts to improve the instrument performance continue in the laboratory. Some goals of this work are to increase the instrument sensitivity by increasing ion throughput, and to improve the instrument response speed and decrease nitric acid background by modifying materials used in the inlet. In the future, we intend to expand the instrument detection capabilities in the negative ion spectrum to include species such as  $\text{H}_2\text{O}$ ,  $\text{HCl}$ , and  $\text{HO}_2\text{NO}_2$ . A second inlet to provide simultaneous sampling of gas and aerosol phases, and a second mass channel for measuring the positive ion spectrum, allowing detection of such compounds as acetone ( $\text{CH}_3\text{COCH}_3$ ) and ammonia ( $\text{NH}_3$ ) are also being discussed.

## References

- Baumgardner D. B., B. J. Huebert and C. Wilson, Extracts from the meeting review, Airborne aerosol inlet workshop, NCAR report TN-362 + 1A, 1991.
- Eisele, F.L. And D. J. Tanner, Ion-Assisted Tropospheric OH Measurements, *Journal Of Geophysical Research-Atmospheres*, 96, 9295--9308, 1991.
- Fahey, D.W., K. K. Kelly, G. V. Ferry, L. R. Poole, J. C. Wilson, D. M. Murphy, M. Loewenstein, And K. R. Chan, In Situ Measurements Of Total Reactive Nitrogen, Total Water, And Aerosol In A Polar Stratospheric Cloud In The Antarctic, *Journal Of Geophysical Research-Atmospheres*, 94, 11299—11315, 1989.
- Hinds, *Aerosol Technology*, John Wiley and sons, 1982.
- Huey, L. G., P. W. Villalta, E. J. Dunlea, D. R. Hanson, and C. J. Howard, Reactions of  $CF_3O^-$  with Atmospheric Trace Gases, *Journal of Physical Chemistry*, 100, 190-194, 1996.
- Huebert, B. J., G. Lee and W. L. Warren, Airborne aerosol inlet passing efficiency measurement, *J. Geophys. Res.*, 95:D10:16369-16381, 1991.
- Knop, G. and F. Arnold, Nitric-Acid Vapor Measurements In The Troposphere And Lower Stratosphere By Chemical Ionization Mass- Spectrometry, *Planetary And Space Science*, 33, 983--986, 1985.
- Knop, G. and F. Arnold, Stratospheric Trace Gas-Detection Using A New Balloon-Borne ACIMS Method - Acetonitrile, Acetone, And Nitric-Acid, *Geophysical Research Letters*, 14, 1262—1265, 1987.
- Mauldin, R.L., D. J. Tanner, and F. L. Eisele, A New Chemical Ionization Mass Spectrometer Technique For The Fast Measurement Of Gas Phase Nitric Acid In The Atmosphere, *Journal Of Geophysical Research-Atmospheres*, 103, 3361--3367, 1998.
- Mohler, O., T. Reiner, And F. Arnold, A Novel Aircraft-Based Tandem Mass-Spectrometer For Atmospheric Ion And Trace Gas Measurements, *Review Of Scientific Instruments*, 64, 1199--1207, 1993.
- Patankar, *Numerical heat transfer and fluid flow*, Taylor and Francis, 1980
- Schlager, H., F. Arnold, D. Hofmann, And T. Deshler, Balloon Observations Of Nitric-Acid Aerosol Formation In The Arctic Stratosphere . I. Gaseous Nitric-Acid, *Geophysical Research Letters*. 17, 1275—1278, 1990.
- Tanner, D.J., A. Jefferson, and F. L. Eisele, Selected Ion Chemical Ionization Mass Spectrometric Measurement of OH, *Journal Of Geophysical Research-Atmospheres*, 102, 6415--6425, 1997.
- Twohy, C. H. and D. Rogers, Airflow and water-drop trajectories at instrument sampling points around the beechcraft king air and lockheed electra, *J. atmos. and oceanic tech.*, 10:566-578, 1993.